

INSTABILITY GROWTH RATE DEPENDENCE ON INPUT PARAMETERS DURING THE BEAM–TARGET PLASMA INTERACTION

MIROSLAV HORKÝ*

Department of Physics, Faculty of Electrical Engineering, Czech Technical University in Prague, Czech Republic

* corresponding author: horkymi1@fel.cvut.cz

ABSTRACT. The two-stream instability without magnetic field is described by the well-known Buneman dispersion relation. For more complicated situations we need to use the Generalized Buneman Dispersion Relation derived by Kulhánek, Břeň, and Bohata in 2011, which is a polynomial equation of 8th order. The maximal value of the imaginary part of the individual dispersion branches $\omega_n(k)$ is very interesting from the physical point of view. It represents the instability growth rate which is responsible for the turbulence mode onset and subsequent reconnection on the ion radius scale accompanied by strong plasma thermalization. The paper presented here is focused on the instability growth rate dependence on various input parameters, such as magnitude of a magnetic field and sound velocity. The results are presented in well-arranged plots and can be used for a survey of the plasma parameters close to which the strong energy transfer and thermalization between the beam and the target occurs.

KEYWORDS: Buneman instability, numerical simulations, plasma, dispersion relation.

1. INTRODUCTION

Two-stream instabilities are the most common instabilities in plasmas which originate on the microscopic scale and which can develop to macroscopic phenomena like a thermal radiation from strong thermalization or non-thermal radiation from reconnections. If we consider that both streams have parallel direction of their velocities, we talk about Buneman instability [1] and if we consider intersecting directions of velocities and anisotropy of temperatures, we talk about Weibel instability [8]. The dispersion relation for two-stream instability without magnetic field in cold plasma is described by the relation

$$\sum_{\alpha=1}^2 \frac{\omega_{p\alpha}}{(\omega - \mathbf{k} \cdot \mathbf{u}_{0\alpha})^2} = 1, \quad (1)$$

where ω is the wave frequency, $\omega_{p\alpha}$ is the plasma frequency of the first and second stream respectively, \mathbf{k} is the wave vector, and $\mathbf{u}_{0\alpha}$ is the vector of the velocity for the first and the second stream respectively.

The most simple situation, in which we can use this relation, is the interaction of two identical streams moving in opposite directions. Equation 1 has simple one dimensional form [4]

$$\frac{\omega_p^2}{(\omega - ku_0)^2} + \frac{\omega_p^2}{(\omega + ku_0)^2} = 1. \quad (2)$$

The two-stream instabilities are usually used for the study of the origin of the observed macroscopic phenomena (e.g. particle acceleration in relativistic plasma shocks [6]). This paper is focused on the general study of the plasma jet interaction on the microscopic scale (not only on the study of one partic-

ular phenomenon origin) and for this case the general dispersion relation is needed. Two generalizations of the two-stream instability dispersion relation were done in last years, first was done by Kulhánek, Břeň and Bohata [5] in 2011 and second was done by Pokhotelov and Balikhin [7] in 2012. In this paper we do all the calculations from [5], because the generalization is more rigorous and precise. The authors called it Generalized Buneman Dispersion Relation (GBDR) and it is described by equation

$$\begin{aligned} \prod_{\alpha=1}^2 \left\{ \Omega_{\alpha}^4 - \Omega_{\alpha}^2 \left[i \frac{\mathbf{F}_{\alpha}^{(0)} \cdot \mathbf{k}}{m_{\alpha}} + c_{s\alpha}^2 k^2 + \omega_{p\alpha}^2 + \omega_{c\alpha}^2 \right] \right. \\ \left. - \frac{\Omega_{\alpha} \omega_{c\alpha}}{m_{\alpha}} \left(\mathbf{F}_{\alpha}^{(0)} \times \mathbf{k} \right) \cdot \mathbf{e}_B \right. \\ \left. + \omega_{c\alpha}^2 (\mathbf{k} \cdot \mathbf{e}_B) \left[i \frac{\mathbf{F}_{\alpha}^{(0)} \cdot \mathbf{e}_B}{m_{\alpha}} + (c_{s\alpha}^2 k^2 + \omega_{p\alpha}^2) \frac{\mathbf{k} \cdot \mathbf{e}_B}{k^2} \right] \right\} \\ - \prod_{\alpha=1}^2 \frac{\omega_{p\alpha}^2}{k^2} \left[\Omega_{\alpha}^2 k^2 - \omega_{c\alpha}^2 (\mathbf{e}_B \cdot \mathbf{k})^2 \right] = 0, \end{aligned} \quad (3)$$

where

$$\Omega_{\alpha} = \omega - \mathbf{k} \cdot \mathbf{u}_{\alpha}^{(0)}, \quad (4)$$

$\omega_{c\alpha}$ is the cyclotron frequency, $\mathbf{F}_{\alpha}^{(0)}$ is the Lorentz magnetic force, \mathbf{e}_B is the unit vector in the direction of magnetic field and $c_{s\alpha}$ is the sound velocity. For $\mathbf{B} = 0$ and cold plasma limit $c_{s\alpha} = 0$, the generalized relation becomes the Eq. 1.

For its analysis it is useful to convert this relation to a non-dimensional form to ensure the scale invariance of the results. The system of coordinates used in the solution is in Fig. 1.

The directions of the vectors \mathbf{u}_α , \mathbf{B} and \mathbf{k} are presented in Fig. 1 in the case of our coordinates system. The wavevector can have any direction, the magnetic field is only in the $(x-z)$ plane and the velocity vectors of the streams are only along the x -axis. These vectors have coordinates

$$\begin{aligned}\mathbf{u}_\alpha &= (u_\alpha, 0, 0), \\ \mathbf{B} &= (B \sin \theta_B, 0, B \cos \theta_B), \\ \mathbf{k} &= (k \cos \varphi \sin \theta_k, k \sin \varphi \sin \theta_k, k \cos \theta_k).\end{aligned}$$

1.1. THE NON-DIMENSIONAL FORM

Non-dimensional variables are defined by relations [2]

$$\begin{aligned}\bar{c}_{s1} &\equiv \frac{c_{s1}}{u_1}, & \bar{c}_{s2} &\equiv \frac{c_{s2}}{u_1}, \\ \bar{\omega}_{c1} &\equiv \frac{\omega_{c1}}{\omega_{p2}}, & \bar{\omega}_{c2} &\equiv \frac{\omega_{c2}}{\omega_{p2}}, \\ \bar{\omega}_{p1} &\equiv \frac{\omega_{p1}}{\omega_{p2}}, & \bar{\omega}_{p2} &\equiv \frac{\omega_{p2}}{\omega_{p2}} = 1, \\ \bar{u}_2 &\equiv \frac{u_2}{u_1}, & \bar{u}_1 &\equiv \frac{u_1}{u_1} = 1, \\ \bar{k} &\equiv \frac{k u_1}{\omega_{p2}}, & \bar{\omega} &\equiv \frac{\omega}{\omega_{p2}},\end{aligned}$$

where index 1 denotes a jet and index 2 denotes a background. Under these definitions, we can convert Eq. 3 into a non-dimensional form [2] which will be

$$\begin{aligned}& \left[\bar{\Omega}_1^4 + i \bar{\Omega}_1^2 \bar{\omega}_{c1} \bar{k} (G_1) - \bar{\Omega}_1^2 (\bar{c}_{s1}^2 \bar{k}^2 + \bar{\omega}_{p1}^2) - \bar{\Omega}_1^2 \bar{\omega}_{c1}^2 \right. \\ & \quad \left. - \bar{\Omega}_1 \bar{\omega}_{c1}^2 \bar{k} (G_3) + (\bar{\omega}_{c1}^2 \bar{k}^2 \bar{c}_{s1}^2 + \bar{\omega}_{c1}^2 \bar{\omega}_{p1}^2) (G_2)^2 \right] \\ & \cdot \left[\bar{\Omega}_2^4 + i \bar{\Omega}_2^2 \bar{\omega}_{c2} \bar{k} \bar{u}_2 (G_1) - \bar{\Omega}_2^2 (\bar{c}_{s2}^2 \bar{k}^2 + 1) - \bar{\Omega}_2^2 \bar{\omega}_{c2}^2 \right. \\ & \quad \left. - \bar{\Omega}_2 \bar{\omega}_{c2}^2 \bar{k} \bar{u}_2 (G_3) + (\bar{\omega}_{c2}^2 \bar{k}^2 \bar{c}_{s2}^2 + \bar{\omega}_{c2}^2) (G_2)^2 \right] \\ & - \left[\bar{\omega}_{p1}^2 (\bar{\Omega}_1^2 - \bar{\omega}_{c1}^2 (G_2)^2) \right] \cdot \left[\bar{\Omega}_2^2 - \bar{\omega}_{c2}^2 (G_2)^2 \right] = 0,\end{aligned}\quad (5)$$

where we denoted

$$\begin{aligned}G_1 &= (\cos \theta_B \sin \varphi \sin \theta_k), \\ G_2 &= (\cos \varphi \sin \theta_k \sin \theta_B + \cos \theta_k \cos \theta_B), \\ G_3 &= (\cos^2 \theta_B \cos \varphi \sin \theta_k - \cos \theta_B \cos \theta_k \sin \theta_B), \\ \bar{\Omega}_1 &= \bar{\omega} - \bar{k} \cos \varphi \sin \theta_k, \\ \bar{\Omega}_2 &= \bar{\omega} - \bar{k} \bar{u}_2 \cos \varphi \sin \theta_k.\end{aligned}$$

The main goal is to find the solution for the $\bar{\omega}$ dependence on \bar{k} . Equation 5 is a polynomial equation of 8th order.

2. NUMERICAL SOLUTION

A classical Newton's algorithm for finding the roots of polynomial equations has one big disadvantage. It does not specify the initial points (points where an algorithm starts the iterations) so it does not guarantee the finding of all the roots. In 2001 Hubbard,

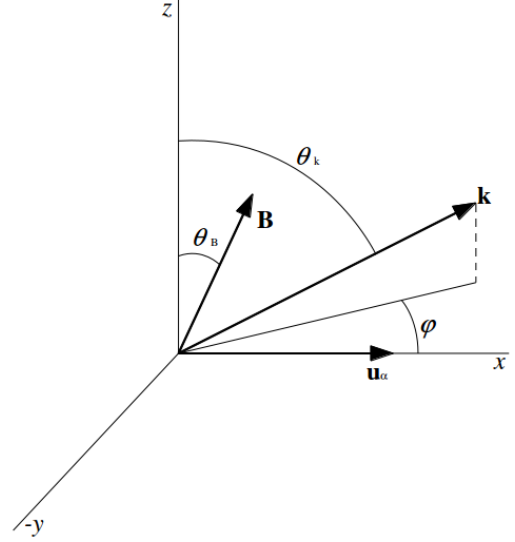


FIGURE 1. System of coordinates used in the simulations.

Schleicher and Sutherland published the article “How to Find All Roots of Complex Polynomials With Newton's Method”, where they demonstrated how to determine the initial points to find all the roots of polynomial equation [3].

2.1. PRINCIPLE OF THE ALGORITHM FUNDAMENTALS

Basic principles are described in [4]. For each \bar{k} we have a polynomial equation of a type

$$c_0 + c_1 \bar{\omega} + c_2 \bar{\omega}^2 + c_3 \bar{\omega}^3 + c_4 \bar{\omega}^4 + c_5 \bar{\omega}^5 + c_6 \bar{\omega}^6 + c_7 \bar{\omega}^7 + c_8 \bar{\omega}^8 = 0. \quad (6)$$

At first we must rescale the polynomial, so we have to find

$$A_{\max} = 1 + \max_k \left\{ \left| \frac{c_k}{c_N} \right| \right\}. \quad (7)$$

From now we will work with the polynomial

$$Q(z) \equiv \sum_{k=0}^N \bar{c}_k z^k, \quad (8)$$

where

$$z \equiv \frac{\bar{\omega}}{A_{\max}}, \quad \bar{c}_k \equiv c_k A_{\max}^k. \quad (9)$$

The second step is to determine the initial points where the algorithm will start the iterations. The net of initial points is determined by radii and angles in the complex plane:

$$r_l \equiv \left(1 + \sqrt{2} \right) \left(\frac{N-1}{N} \right)^{(2l-1)/4L}, \quad (10)$$

$$l = 1, \dots, L, \quad (11)$$

$$L \equiv \lceil 0.26632 \ln N \rceil, \quad (12)$$

$$\xi_m \equiv \frac{2\pi m}{M}, \tag{13}$$

$$m = 0, \dots, M - 1, \tag{14}$$

$$M \equiv \lceil 8.32547N \ln N \rceil. \tag{15}$$

Then the net of initial points is

$$z_{lm} = r_l \exp(i\xi_m), \tag{16}$$

$$l = 1, \dots, L, \tag{17}$$

$$m = 0, \dots, M - 1. \tag{18}$$

The initial net of points has definitely LM numbers. From these numbers the algorithm starts the iterations. A number of iterations O is defined by accuracy ε by the definition

$$O \equiv \left\lceil \frac{\ln(1 + \sqrt{2}) - \ln \varepsilon}{\ln N - \ln(N - 1)} \right\rceil. \tag{19}$$

The bracket $\lceil x \rceil$ means the ceiling function (first integer number which is higher or equal to x). Solutions which do not accomplish $|Q(z_o) < \varepsilon|$ are not the roots of the polynomial.

After finding all the roots in the rescaled polynomial we have to do the backscaling

$$\bar{\omega}_o = A_{\max} z_o. \tag{20}$$

2.2. EXAMPLE OF THE SOLUTION

The first numerical solution was made in [5] for the situation of two identical opposite plasma beams in a magnetic field. This example of dispersion branches is for more complicated situation – one plasma beam penetrates into the plasma background and magnetic field has both perpendicular and parallel components. The parameters of this simulation are in Tab. 1 and graphical result is in Fig. 2.

The result is depicted in well arranged plot where blue dots represent real branches and red dots imaginary branches of the solution. Also maximal value of the imaginary branch which is so called Plasma Instability Growth Rate (PIGR) is depicted with sign “Max”.

| Parameter | Value |
|---|---------|
| $\bar{\omega}_{c1} = \bar{\omega}_{c2}$ | 0.5 |
| $\bar{c}_{s1} = \bar{c}_{s2}$ | 0.1 |
| \bar{u}_2 | 0 |
| $\bar{\omega}_{p1}$ | 1 |
| θ_k | $\pi/2$ |
| φ | 0 |
| θ_B | $\pi/4$ |

TABLE 1. Parameters used in example of the solution.

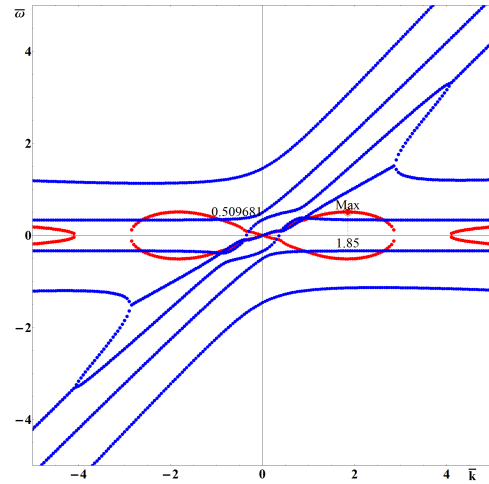


FIGURE 2. Example of solution of the GBDR with marked maximal value of imaginary part.

3. PIGR DEPENDENCE ON VARIOUS INPUT PARAMETERS

3.1. DEPENDENCE ON CYCLOTRON FREQUENCIES

At first the PIGR dependence on both jet and the background cyclotron frequencies was found.

3.1.1. RESULTS FOR $\bar{\omega}_{c1}$

The parameters used in the simulations are presented in Tab. 2 and the results are depicted in Fig. 3. It is obvious that the PIGR grows linearly from the value $\bar{\omega}_{c1} = 0.6$.

| Parameter | Value |
|-------------------------------|--------------------------|
| $\bar{\omega}_{c1}$ | $\langle 0.5, 3 \rangle$ |
| $\bar{\omega}_{c2}$ | 0.5 |
| $\bar{c}_{s1} = \bar{c}_{s2}$ | 0.1 |
| \bar{u}_2 | 0 |
| $\bar{\omega}_{p1}$ | 1 |
| θ_k | $\pi/2$ |
| φ | 0 |
| θ_B | $\pi/4$ |

TABLE 2. Parameters used in the simulations with various parameter $\bar{\omega}_{c1}$.

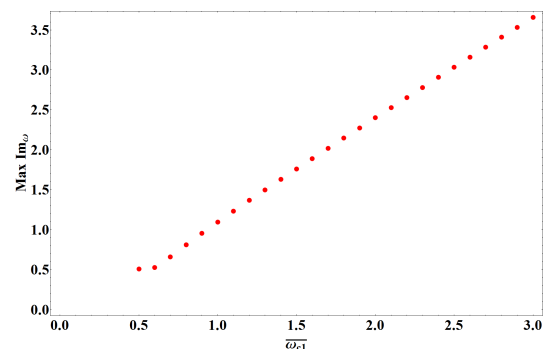


FIGURE 3. The PIGR dependence on $\bar{\omega}_{c1}$.

3.1.2. RESULTS FOR $\bar{\omega}_{c2}$

The parameters used in the simulations are presented in Tab. 3 and the results are shown in Fig. 4.

From these results we can see the local minimum of PIGR which origins due to the bifurcation of the solution. The bifurcation is depicted in three dimensional plot where the first axis is k , second is $\bar{\omega}$ and third is $\bar{\omega}_{c2}$ (see the Fig. 5).

| Parameter | Value |
|-------------------------------|--------------------------|
| $\bar{\omega}_{c1}$ | 0.5 |
| $\bar{\omega}_{c2}$ | $\langle 0.5, 3 \rangle$ |
| $\bar{c}_{s1} = \bar{c}_{s2}$ | 0.1 |
| \bar{u}_2 | 0 |
| $\bar{\omega}_{p1}$ | 1 |
| θ_k | $\pi/2$ |
| φ | 0 |
| θ_B | $\pi/4$ |

TABLE 3. Parameters used in the simulations with various parameter $\bar{\omega}_{c2}$.

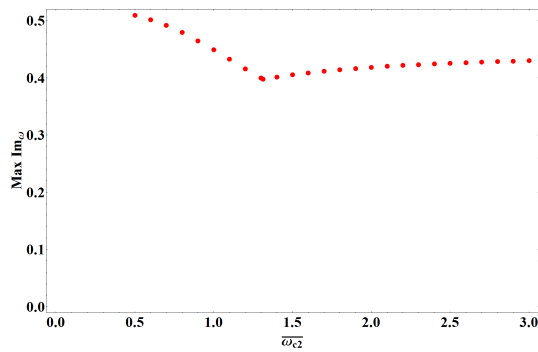


FIGURE 4. The PIGR dependence on $\bar{\omega}_{c2}$.

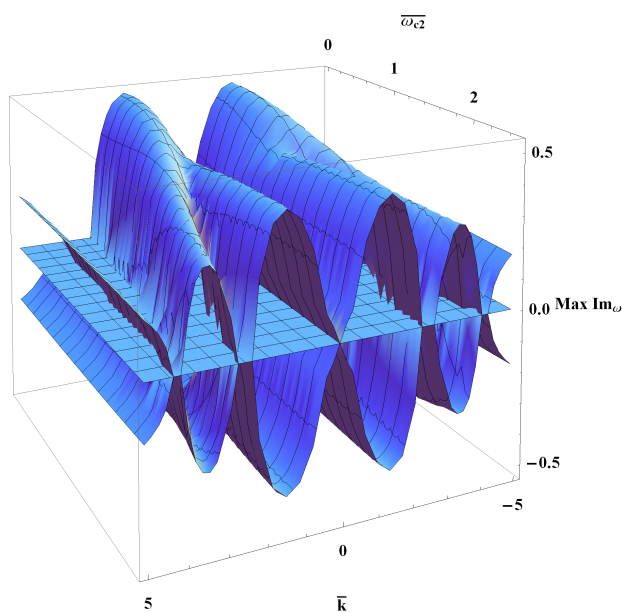


FIGURE 5. Imaginary part of the solution in three dimensions with an observable bifurcation.

3.2. DEPENDENCE ON SOUND VELOCITIES

Subsequently the PIGR dependence on both jet and the background sound velocities was found.

3.2.1. RESULTS FOR \bar{c}_{s1}

The parameters used in the simulations are presented in Tab. 4 and the results are depicted in Fig. 6.

| Parameter | Value |
|---------------------|--------------------------|
| $\bar{\omega}_{c1}$ | 0.5 |
| $\bar{\omega}_{c2}$ | 0.5 |
| \bar{c}_{s1} | $\langle 0.1, 2 \rangle$ |
| \bar{c}_{s2} | 0.1 |
| \bar{u}_2 | 0 |
| $\bar{\omega}_{p1}$ | 1 |
| θ_k | $\pi/2$ |
| φ | 0 |
| θ_B | $\pi/4$ |

TABLE 4. Parameters used in the simulations with various parameter \bar{c}_{s1} .

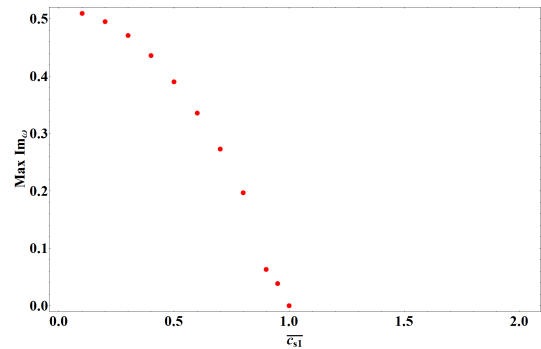


FIGURE 6. The PIGR dependence on \bar{c}_{s1} .

It is obvious that after value $\bar{c}_{s1} = 1$, there is no imaginary branch of the solution, so there are not any instabilities.

3.2.2. RESULTS FOR \bar{c}_{s2}

The parameters used in the simulations are presented in Tab. 5 and the results are depicted in Fig. 7.

Figure 7 presents a similar bifurcation point like in Fig. 4.

| Parameter | Value |
|---------------------|----------------------------|
| $\bar{\omega}_{c1}$ | 0.5 |
| $\bar{\omega}_{c2}$ | 0.5 |
| \bar{c}_{s1} | 0.1 |
| \bar{c}_{s2} | $\langle 0.1, 1.5 \rangle$ |
| \bar{u}_2 | 0 |
| $\bar{\omega}_{p1}$ | 1 |
| θ_k | $\pi/2$ |
| φ | 0 |
| θ_B | $\pi/4$ |

TABLE 5. Parameters used in the simulations with various parameter \bar{c}_{s2} .

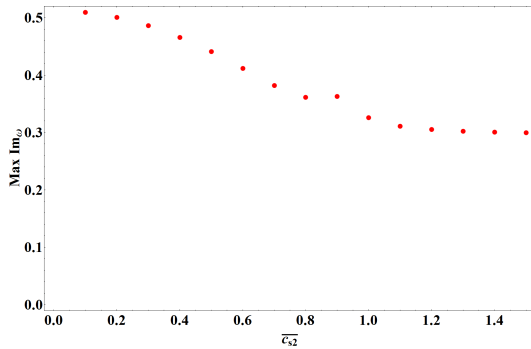


FIGURE 7. The PIGR dependence on \bar{c}_{s2} .

3.3. RESULTS OVERVIEW

We found the PIGR dependence on four parameters $\bar{\omega}_{c1}$, $\bar{\omega}_{c2}$, \bar{c}_{s1} , and \bar{c}_{s2} . The main dissimilarity between the dependencies on the cyclotron frequencies is caused by zero velocity of the background. Since the jet has non-zero velocity with a component perpendicular to the magnetic field, the jet particles react to the change of the magnetic field more strongly than the background particles. The dissimilarity between the dependencies on the sound velocities has the same origin. Because of the non-zero velocity of the jet, the jet could be subsonic and therefore it could be in the state with no instabilities.

4. CONCLUSIONS AND FUTURE WORK

First of all, the GBDR was converted into a non-dimensional form which ensures the scale invariance of the problem, which means that the results can be used both for the laboratory and astrophysical plasmas. Afterwards the dispersion relation had been solved for the angular frequency via the algorithm suggested by Hubbard, Schleicher, and Sutherland. In every solution branch there were separated real and imaginary parts and subsequently found plasma instability growth rate numerically. Finally, the PIGR dependence on four input parameters $\bar{\omega}_{c1}$, $\bar{\omega}_{c2}$, \bar{c}_{s1} and \bar{c}_{s2} was found. All these numerical calculations

were done on microscopic scale and in the linear approximation. These results can be used for lookup of the plasma parameters close to which the strong energy transfer and thermalization between the beam and the target occurs which will be the first part of the future work. Another part will be Particle In Cell simulations of plasma turbulences origin in the vicinity of PIGR maximum.

ACKNOWLEDGEMENTS

Research described in the paper was supervised by Prof. P. Kulháněk from the FEE CTU in Prague and supported by the CTU grants SGS10/266/OHK3/3T/13, SGS12/181/OHK3/3T/13.

REFERENCES

- [1] O. Buneman. Dissipation of currents in ionized media. *Phys Rev* **115**(3):503–517, 1959.
- [2] M. Horký. Numerical solution of the generalized Buneman dispersion relation. In *Proceedings of Poster 2012*. Prague, 2012.
- [3] J. Hubbard, D. Schleicher, S. Sutherland. How to find all roots of complex polynomials with Newton’s method. *Inventiones Mathematicae* **146**:1–33, 2001.
- [4] P. Kulhanek. *Uvod to teorie plazmatu*. AGA, Prague, 1st edn., 2011. (in Czech).
- [5] P. Kulhanek, D. Bren, M. Bohata. Generalized Buneman dispersion relation in longitudinally dominated magnetic field. *ISRN Condensed Matter Physics* **2011**, 2011. Article id 896321.
- [6] I. Nishikawa, K., P. Hardee, B. Hededal, C., et al. Particle acceleration, magnetic field generation, and emission in relativistic shocks. *Advances in Space Research* **38**:1316–1319, 2006.
- [7] A. Pokhotelov, O., A. Balikhin, M. Weibel instability in a plasma with nonzero external magnetic field. *Ann Geophys* **30**:1051–1054, 2012.
- [8] E. S. Weibel. Spontaneously growing transverse waves in a plasma due to an anisotropic velocity distribution. *Phys Rev Lett* **2**(3):83–84, 1959.